AN ANODELESS (BARE) TETHER EXPERIMENT

J.R. Sanmartín, E. Ahedo, L. Conde, F. Ibáñez, and J. Peláez
E.T.S.I. Aeronáuticos, Universidad Politécnica
28040 Madrid, Spain

Introduction

NETT (New Electrodynamic Tether Technology) is an experiment proposed to ESA in 1991 as part of the Columbus Precursor Flights. It was originally intended to fly as an exposed payload in the Shuttle cargo bay. The main purpose was to demonstrate the electrodynamical capabilities of the innovative "bare tether" concept. The proposed conceptual design was recommended by a Scientific Panel of ESA, meeting in Heidelberg in March 1992. Unfortunately, the Precursor Flights have all but been scuttled, particularly as far as exposed payloads are concerned. The experiment, horever, is being considered in accomodation studies (APLSS, PIERS) for the European modulus of the future Space Station. Additionally, it might be possible to fly the bare tether in a Russian spacecraft.

Standard contactors

The standard (insulated) electrodynamic tether design has a basic drawback: the end contactors, that establish and control the charge exchange with the ionosphere, may have large impedances. The anodic (electron collecting) contactor is the major problem, as it is difficult to collect a substantial current from the rarefied ionosphere. As an example, the big metallic sphere (radius $R = 0.8m$) acting as anode in the italo-american TSS-1, 20km tether might collect a current $0.1 - 0.2A$.

The generic problem is the small thermal current density, $J_{th} \sim 10^{-3} A/m^2$. Defining an effective collecting area as the ratio of current I_l to thermal current density, $A_{eff} \equiv I_l/J_{th}$, a representative value, $I_l \sim 10A$, would require $A_{eff} \sim 10^4 m^2$. Clearly, one needs both a large anode and a large area gain,

$$G \equiv A_{eff}/\text{Anodic area} \equiv I_l/J_{te} \times \text{Anodic area}.$$

A passive contactor gets its gain from a bias voltage ϕ_A. Since the electron temperature T_e is about $0.1eV$, $e\phi_A/T_e$ is easily large. Nonetheless, it is difficult to obtain a substantial gain because the electron thermal gyroradius l_e is small ($l_e \sim 20mm$), resulting in significant magnetic guiding; also, the electron Debye length λ_D is so small ($\lambda_D \sim 5mm$) that electric shielding is very effective. The gain $G(e\phi_A/T_e, R/\lambda_D, R/l_e)$ comes out to be weak.

An active contactor emits an ion current, I_i, so as to reduce the shielding due to the attracted electrons. In addition, the relative motion of attracted electrons and emitted ions should produce plasma turbulence, scattering electrons off magnetic field lines. Since emitted ions are accelerated through the same potential difference as attracted electrons, the characteristic density ratio, measuring the degree of charge quasineutrality, is $n_i(emit)/n_e(attr.) \sim \sqrt{m_i/m_e} I_i/I_l$, and the gain becomes

$$G \equiv G\left(\frac{e\phi_A}{T_e}, \frac{R}{\lambda_D}, \frac{R}{l_e}, \frac{I_i}{I_l}\sqrt{\frac{m_i}{m_e}}\right).$$

However, the space charge of the emitted ions limits I_i itself, the maximum gain being low.

Proposed active contactors circumvent this problem by ejecting a plasma. Emitted electrons keep around the contactor and provide quasineutrality. There are at present, however, gross uncertainties in the theory of plasma contactors. Besides, it is extremely difficult to simulate ionospheric conditions with laboratory contactors. For an intensity,

$I_l \sim 10A$ the effective contactor radius R_{eff} is above $15m$, and $R_{eff}/l_e \sim 10^3$, $R_{eff}/\lambda_D \sim 3\times 10^3$. Actual experiments, on the other hand, reach values $R_{eff}/l_e \sim 10$, $R_{eff}/\lambda_D \sim 100$. The scaling of the contactor is even more difficult. Space experiments on contactors (PMG, Volcano Project) should thus be quite helpful [Ahedo et al., 1992].

A bare tether anode

A passive anodic contactor might work if it presents two disparate, characteristic lengths, as in the case of an elongated cylinder, with length $L_B >> R$. No matter how small R, one could have a large anodic area, $2\pi R L_B$, for large enough L_B. The collection, on the other hand, is governed by the strongest gradients, and it will be approximately two dimensional. For R small enough, there will be no magnetic or shielding effects (OML regime). The area gain is then $G \simeq G(e\phi_A/T_e, R/\lambda_D \simeq 0, R/l_e \simeq 0) \simeq (4e\phi_A/\pi T_e)^{1/2} \gg 1$.

Actually, in $2D$ (but not in $3D$) geometry, R/λ_D need not be small in order to have the OML regime; here, it suffices to have $R < 10mm$. A somewhat less definite statement holds for R/l_e. Magnetic guiding results in a known canonical bound that I_l cannot exceed. In $2-D$ geometry the OML current gets well below this bound for $R < l_e (\sim 20mm$ here) and $e\phi_A/T_e$ large, suggesting that magnetic effects are negigible. (It is the other way around in $3-D$ geometry. [Sanmartín et al., 1993].)

Note that a segment of length L_B coming out positively biased in a fully bare tether of total length L_t, might serve as anode. Ions would then be collected over the length $L_t - L_B$. Both the electron current into L_B and the ion current into $L_t - L_B$ are in the OML regime, and we find

$$\frac{I(\text{ions})}{I(\text{electrons})} \sim \left(\frac{m_e}{m_i}\right)^{1/2} \left(\frac{L_t - L_B}{L_B}\right)^{3/2} .$$

Too small a fraction L_B/L_t reduces both the net current $I_l = I$ (electrons) $-I$ (ions) reaching the load impedance Z_l at the cathodic end, and the load power $Z_l I_l^2$. For L_B/L_t too large, on the other hand, the large anodic impedance would reduce the generator efficiency. There exists, therefore, an optimal bare tether, which is found to have $I(\text{ions})/I(\text{electrons}) \sim L_B/L_t$ leading to $L_B/L_t \sim (m_e/m_i)^{1/5} \sim 1/7$.

Consider an ideal tether, having no contactor or wave impedance. It obeys the simple circuit equation

$$\varepsilon = (Z_l + Z_t) I_l \quad , \qquad [\varepsilon \equiv VBL_t \quad , \quad Z_t \equiv L_t/\sigma_t A_t] \quad ,$$

with $V \equiv$ orbital speed, $B \equiv$ geomagnetic field, $\sigma_t \equiv$ tether conductivity, $A_t \equiv$ tether cross section. It then follows

$$\frac{Z_l I_l^2}{\varepsilon^2/Z_t} = \frac{Z_l/Z_t}{(1 + Z_l/Z_t)^2} \quad ,$$

which is the usual expression for load to short-circuit power ratio, with a $1/4$ maximum at $Z_l/Z_t = 1$. This can be rewritten as

$$\frac{Z_l I_l^2}{(VB)^2 \sigma_t A_t L_t} = \frac{Z_l I_l^2}{\varepsilon I_l}\left(1 - \frac{Z_l I_l^2}{\varepsilon I_l}\right)$$

which can be read as

$$\text{Load Power/Normalized Mass} = \text{Efficiency}(1 - \text{Efficiency}).$$

The above equation is compared with the corresponding relation for an optimal anodeless, bare tether in Fig. 1 [Sanmartín et al., 1993]. To determine optimal values for L_t and

$A_t \equiv \pi R^2$ (for a desired load power) one naturally must make a trade-off choice between efficiency and load power per unit mass of tether. A 0.75 efficiency appears as a reasonable choice. An optimal design assumes given values for B and ionospheric density. Figure 2 shows the decrease in efficiency when density and magnetic field differ from those assumed in the proposed experiment.

For a fixed value of efficiency the load power scales as the full power lost in the magnetic braking, which is $\varepsilon \times I_l \propto L_t \times RL_B^{3/2} \propto L_t^{5/2} R$. Also, for a fixed value of load power per unit mass, the load power scales as the tether mass $\propto L_t R^2$. One thus obtains

$$L_t \propto (\text{Load Power})^{1/4} \quad , \quad R \propto (\text{Load Power})^{3/8}.$$

The NETT experiment

The experiment proposed to ESA involves both a technology demonstration and scientific experiments (artificial auroral effects, ELF emission). It uses an optimal bare tether with 1Kw of load power, $0.87A$ load current, $1.15mm$ diameter and $7.5km$ length. Work being carried out includes analysis of the dynamics of tether deployment; experiments to design and develop an active cathodic (electron ejecting) contactor; and analytical studies on models for the cathodic contactor and wave radiation (particularly the wave impedance). A Phase-B engineering study has just been carried out by Alcatel Space (France) to identify critical issues, develop a deployment mechanism and get an overall baseline design.

Dynamical analysis

The main objective of this dynamical analysis is to obtain an open loop strategy for the deployment that leaves out the tether aligned with the vertical, at rest, that is, without later libration. Moreover, we try to minimize the deployment time.

The deployment is carried out here taking into account several common simplifying assumptions in order to pinpoint the essential aspects of the dynamics (the orbiter is in a circular orbit; only in-plane stable motion is considered; the tether is flexible, nonextensible, etc). A light tether holds a rectilinear shape during the deployment and the tension does not vary along the tether. In this approximation, it is only necessary to know the position of the end mass A; the evolution of its polar coordinates (l, θ) is given by the following nondimensional equations:

$$\ddot{l} - l\{\dot{\theta}^2 + 2\dot{\theta} + 3\cos^2\theta\} = -\hat{T}(\tau) \tag{1}$$

$$\ddot{\theta} + \frac{2\dot{l}}{l}(1 + \dot{\theta}) + \frac{3}{2}\sin 2\theta = 0 \tag{2}$$

which must be integrated with the appropriate initial conditions: (at $\tau = 0$: $l = 0$, $\dot{l} = 1$, $\theta = \varphi_0$, $\dot{\theta} = -1$) where $\tau = 0$ has been taken as the epoch in which the deployment begins (the end mass is ejected from the orbiter). The nondimensional variables used are: $\tau = \omega t$, $l = \omega L / v_A$, $\hat{T}(\tau) = T(\tau)/\omega m_A v_A$ where L is the tether length, $m_A v_A$ is the ejected momentum of the end mass and $\omega = 2\pi/P$ (P is the orbital period of the orbiter).

These equations are the linear momentum equations for the end mass A when acted upon by: the gravity gradient force, the inertial Coriolis force, and the tension $T(t)$ imposed at the orbiter end of the tether and transmitted to the end mass. Therefore, the in-plane motion of the end mass depends on the following control parameters: *i)* ejection velocity V_A, *ii)* ejection angle φ_0, *iii)* the tether tension $T(t)$.

Our deployment process [Peláez, 1994 a, b] has two different phases: *i)* Uniform deployment, $\dot{l}$ = constant, and *ii)* Exponential deployment, $\dot{l}/l$ = constant (see fig. 3). During the first phase the tension is low, and the gravity gradient is small; the end mass goes away from the orbiter (backward motion) and the gravity gradient grows; however, at certain

moment it is necessary to put the tether in tension, because the dominant Coriolis force must be reduced to avoid the tether revolving around the orbiter. The exponential phase begins then, and the tether tension brakes the deployment and reduces the Coriolis force, but it does not stop the end mass because then the gravity gradient is sufficiently large.

The values of $l_0, \dot{l}_0, \theta_0$ and $\dot{\theta}_0$ at τ_0 the end of the first stage, are the initial conditions from which the exponential one begins. The deployed length grows, in agreement with:

$$\dot{l}/l = C_0 \qquad \Rightarrow \qquad l(\tau) = l_0 \exp\{C_0(\tau - \tau_0)\}.$$

For such a deployment the tension $\hat{T}(\tau)$ follows from (1) where $\theta(\tau)$ is given by integrating (2) from the initial conditions: $\tau = \tau_0 : \ \theta(\tau_0) = \theta_0, \ \dot{\theta}(\tau_0) = \dot{\theta}_0$ (notice: in (2) $\dot{l}/l = C_0$ now).

For $C_0 < 3/4$ there are four steady solutions; two are stable and one of these, $\theta = \theta_1$, is upward (the tether deploys following a radial straight line corresponding to the initial conditions: $\theta(\tau_0) = \theta_1, \ \dot{\theta}(\tau_0) = 0$). Such a solution appears as an stable focus in the phase plane $(\theta, \dot{\theta})$ (see fig. 4). To approach that solution, initial conditions must lie inside its attraction domain (the tether swings around this radial line $\theta = \theta_1$ while deploying). Due to the very hard contraction of the "volume" in the phase plane, all trajectories of the attraction domain cross the segment $\bar{PQ}$ of fig. 4; when C_0 ranges in the interval $I = [0.2454, 0.3662]$ the origin $(\theta = 0, \dot{\theta} = 0)$ lies in the segment $\bar{PQ}$. Therefore, there is a trajectory (A) that goes into the origin of the phase plane. If the final conditions of the first stage lie in this particular trajectory, the conditions: $\theta = \dot{\theta} = 0$ will be reached in a certain moment; if the deployment is then stopped the tether will leaves out aligned with the vertical and without libration (at rest).

The first stage ends when the ratio $\dot{l}/l$ reaches the value C_0 previously fixed: $\frac{\dot{l}}{l} = \frac{1}{\tau} = C_0 \quad \Rightarrow \quad \tau = \frac{1}{C_0}$. For each value of C_0 in the interval I there is a critical value of the ejection angle: $\varphi_0^* = \varphi_0^*(C_0)$ for which, at the end of the second stage, the following conditions: $\theta_f = \dot{\theta}_f = 0$ are reached (C_0 must be in the interval $[0.343, 0.366]$). Let l_f be this final value of the non-dimensional tether length corresponding to the critical ejection angle $\varphi_0^*(C_0)$; it is possible then to obtain the ejection velocity needed for such a deployment from the relation (notice that any tether's length can be deployed adjusting the ejection velocity):

$$V_A = \omega L / l_f.$$

Contactor experiments

The maximum amount of contactor current transferred could be limited by the development of double layers in the nearby plasma. These stable potential structures [Williams and Wilbur et al., 1989, 1991] consist in a continuous spatial variation of the plasma potential from the high density emitted plasma plume up to the cold ambient plasma. In a hollow cathode, this spatial profile is complicated in the front of the contactor by the ionization of the remanent neutral gas within the plasma plume. It has been postulated that this relative high ionization rate could be responsible for the plasma potential hill structures observed in the region close to the plasma contactor. The resulting plasma potential profile resembles closely those of so called *triple layers* [Allen, 1985] which are sustained by trapped electronic populations . This could result in a limitation in the charge transport performance of these devices.

In the UPM plasma facility we have investigated these ionization induced effects in a simple experiment of current collection. The experimental device and procedures have been described elsewere [Conde and León, 1994]. Briefly, the neutral pressures were kept high in order to enhance the ionization (4-6 $\times$ 10^{-3} Torr) and low amounts of neutral gas (1-8 $\times$ 10^{-2} sccm) introduced later into a small cilindrical cavity. A glow discharge was produced between the walls of a (100 liters) metallic chamber and this anodic cavity.

Then, the electrons present in the plasma are focused into the inner face of the cilinder and confronted with the neutral gas flow. This later plays an analogous role to the remanent neutral gas emitted by the hollow cathode. In these conditions, stable multiple DLs with spherical symmetry develop in the main volume of the gas discharge, and typical plasma potential and density profiles are shown in Fig. 5.

As it may be appreciated, the structure is marked by of succesive plasma potential leaps and the appearance at the anodic side of each double layer, where plasma quasineutrality is not satisfied. The electronic density falls at these points, indicating an excess of positive charge. Conversely, the electronic temperature grows at the catodic side of the double layer because of the acceleration of electrons across the plasma potential drop. Similar structures composed by a single double layer have been reported when a positive biased electrode, inmersed in a plasma, is polarized above the ionization potential of the neutral gas.

The essential mechanism for generation of charges in the volume of glow discharge is electron impact. Afther the ionization of a neutral atom, the secondary electron generated would move fast towards the anode because of the drift motion induced by the electric field, which corresponds to the electron collection process. On the contrary, the massive ions would be left behind, creating a region in which the ion density is greater. This would explain the fall in the electronic density in Fig. 5 at the high potential side of each double layer [Williams and Wilbur et al., 1989, 1991].

Contrary to the case of hollow cathodes, the high density plasma plume is absent in our experiments, but the succesive potential hills are also present in the plasma potential profile. Therefore, the increment of the local volume ionization rate would suffice for the increase of plasma potential at the high potential edge of a double layer. These results would confirm the possible influence of ionization in the generation of the plasma potential hills in the front of double layers formed in hollow cathodes [Williams and Wilbur et al., 1989, 1991].

References

E. Ahedo, J.R. Sanmartín and M. Martínez-Sánchez , in Physics of Charged Bodies in Space Plasmas, pp. 1-8, Societá Italiana di Fisica, Bologna (1992); also, *Physics of Fluids* B 4, 3847 (1992).

J.R. Sanmartín, E. Ahedo and M. Martínez-Sánchez , in Physics of Charged Bodies in Space Plasmas, pp. 201-208, Societá Italiana di Fisica, Bologna (1992); also, *J. Propulsion and Power* 9, 353 (1992).

J.E. Allen , *Plasma Phys. and Controlled Fusion.*, **27**, (12), 1343, (1985).

L. Conde and L. León , *Phys. of Plasmas*, (accepted).

J. Peláez , *Acta Astronautica* (submitted, 1994 a).

J. Peláez , *Acta Astronautica* (submitted, 1994 b).

John D. Williams , *Plasma Contactor Research,* P.J. Wilbur, ed. NASA CR-187097, (1991), NASA CR-182283, (1989).

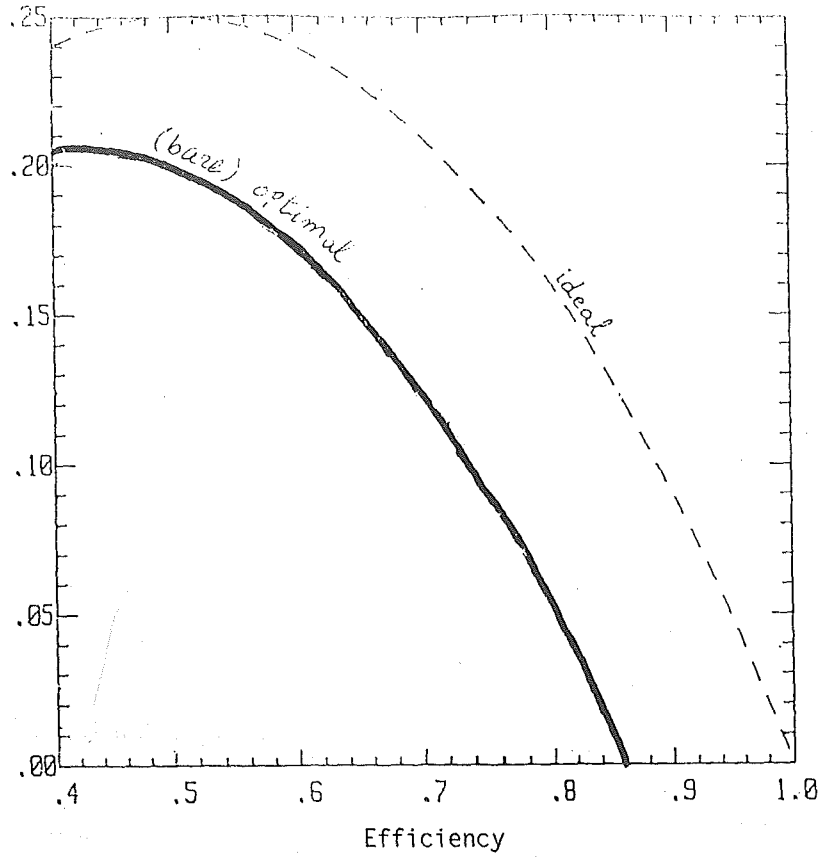
.25
.20
.15
.10
.05
.00
.4
.5
.6
.7
.8
.9
1.0
(bare) optimal
ideal
Load Power
Normalized Mass
Efficiency

FIG.1

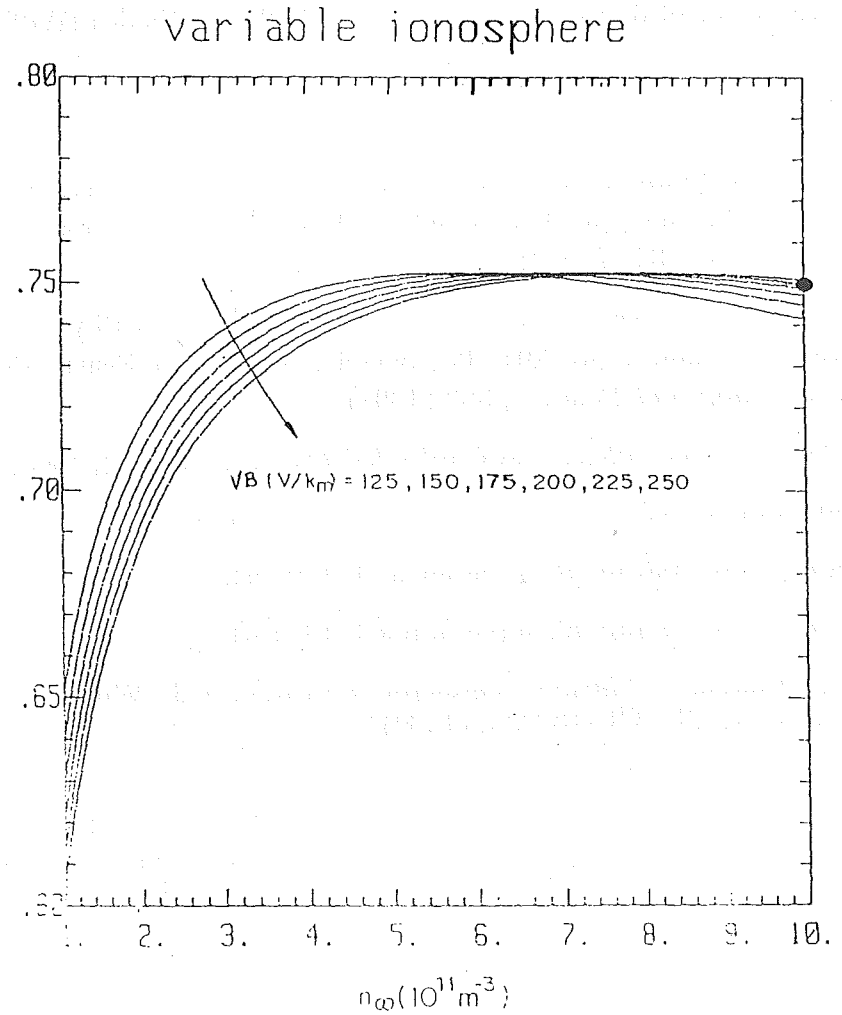
variable ionosphere
.80
.75
.70
.65
2.
3.
4.
5.
6.
7.
8.
9.
10.
VB (V/km) = 125, 150, 175, 200, 225, 250
Efficiency
$n_\omega(10^{11}m^{-3})$

FIG. 2

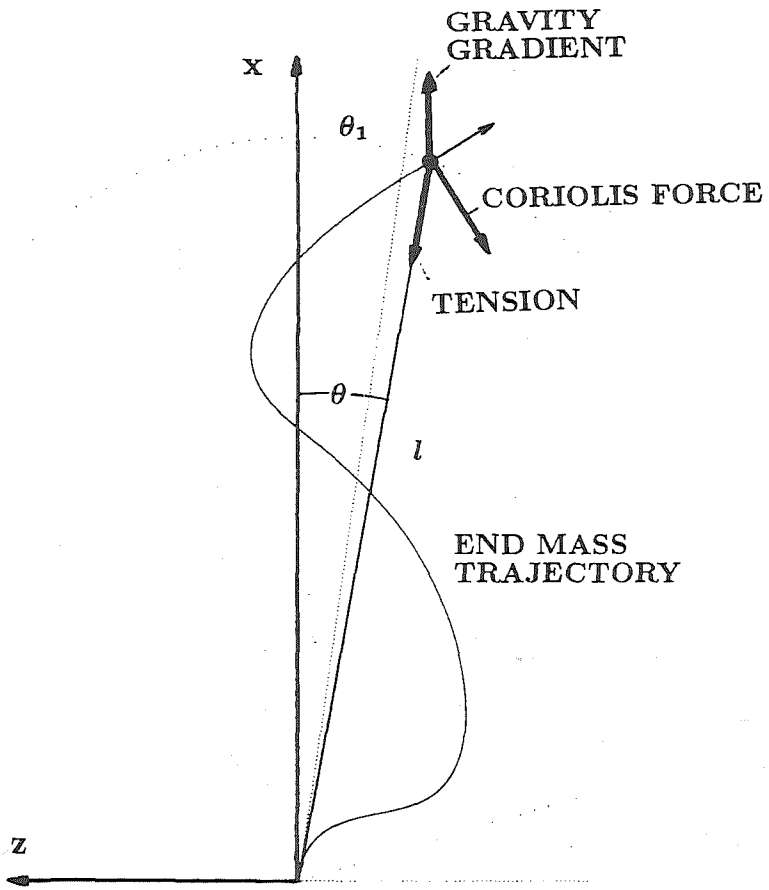
GRAVITY
GRADIENT
x
θ_1
CORIOLIS FORCE
TENSION
θ
l
END MASS
TRAJECTORY
z

Fig. 3

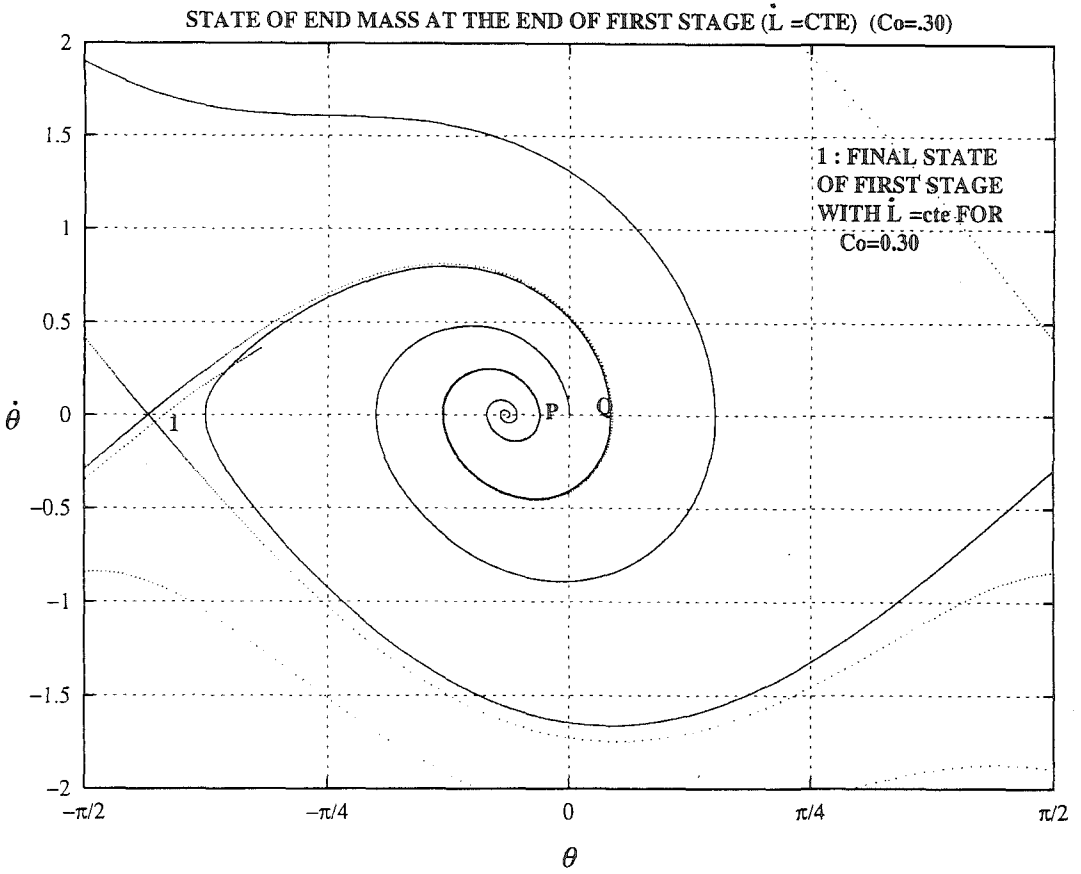
STATE OF END MASS AT THE END OF FIRST STAGE ($\dot{L}$ =CTE) (Co=.30)
1 : FINAL STATE
OF FIRST STAGE
WITH $\dot{L}$ =cte FOR
Co=0.30
P
Q
1
2
1.5
1
0.5
0
−0.5
−1
−1.5
−2
$\dot{\theta}$
−π/2
−π/4
0
π/4
π/2
θ

Fig. 4

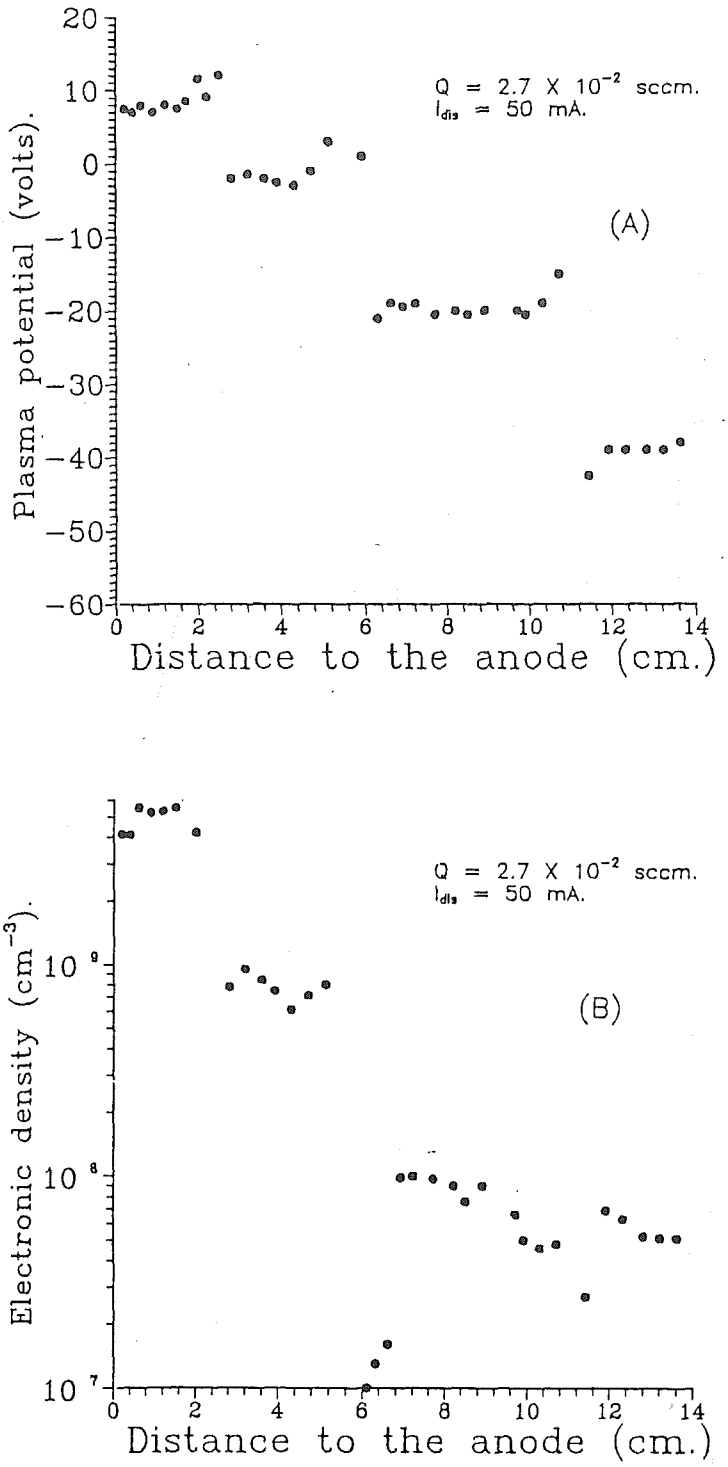

FIGURE 5

Values of the plasma potential (A) and electronic density (B) along the axis of simmetry of the multiple double layer structure. The location of the double layers corresponds to the jumps in the plasma potential.